IOP Publishing New J. Phys. 26 (2024) 013004 https://doi.org/10.1088/1367-2630/ad15b5

New Journal of Physics
The open access journal at the forefront of physics

Deutsche Physikalische Gesellschaft DPG
IOP Institute of Physics

Published in partnership with: Deutsche Physikalische Gesellschaft and the Institute of Physics

CrossMark

OPEN ACCESS

RECEIVED
9 August 2023

REVISED
8 December 2023

ACCEPTED FOR PUBLICATION
14 December 2023

PUBLISHED
5 January 2024

PAPER

Parity-enhanced quantum optimal measurements

Hai-Jun Xing[1,2], **Libin Fu**[2,*] **and Su Yi**[3,4,5,*]

[1] Center for Quantum Sciences and School of Physics, Northeast Normal University, Changchun 130024, People's Republic of China
[2] Graduate School of China Academy of Engineering Physics, Beijing 100193, People's Republic of China
[3] CAS Key Laboratory of Theoretical Physics, Institute of Theoretical Physics, Chinese Academy of Sciences, Beijing 100190, People's Republic of China
[4] School of Physical Sciences & CAS Center for Excellence in Topological Quantum Computation, University of Chinese Academy of Sciences, Beijing 100049, People's Republic of China
[5] Peng Huanwu Collaborative Center for Research and Education, Beihang University, Beijing 100191, People's Republic of China
[*] Authors to whom any correspondence should be addressed.

E-mail: lbfu@gscaep.ac.cn and syi@itp.ac.cn

Keywords: quantum precision measurement, optimal measurement, parity measurement, parity symmetry

Abstract

In quantum metrology, measurement and estimation schemes are vital for achieving higher precision, along with initial state preparation. This article presents the compound measurement of parity and particle number, which is optimal for a broad range of states named *equator states* (ESs). ES encompasses most pure input states used in current studies and, more significantly, a wide range of mixed states. Moreover, the ES can be prepared directly using non-demolition parity measurement. We thus propose an improved quantum phase estimation protocol applicable to arbitrary input states, ensuring precision consistently surpassing that of the standard protocol. The proposed scheme is also demonstrated using a nonlinear interferometer, with the realization of the non-demolition parity measurement in atomic condensates.

1. Introduction

Parameter estimation lies at the heart of the interferometries. In typical interferometry setups, parameters are encoded into the sensor's input state and later inferred from the measurement results through suitable estimators [1–5]. The estimation precision is upper bounded by quantum Cramér–Rao (CR) inequality, in terms of the quantum Fisher information (QFI) [1–5]. It is known that CR bound can be significantly increased by utilizing quantum resources, such as entanglement and squeezing [3–16]. The quantum-enhanced measurement precision has been experimentally demonstrated in various systems [17–23] and has also been applied to the estimates of time [24–28], magnetic field [29–32], gravitational field [33, 34], and gravitational wave [35–38].

Nevertheless, saturating the upper CR bound still requires elusive optimal measurements (OMs) and a suitable estimation scheme [1, 2, 39, 40]. Generally speaking, OMs depend on the states of the system and even on the value of the parameter under estimation [1, 2, 39, 40]. Consequently, OMs are usually achieved via feeding back the estimated parameter and updating the measurement adaptively [41, 42]. For the two most commonly used measurements, number counting and parity [43, 44], in quantum metrology, there have been extensive theoretical and experimental studies on their optimality. Parity measurement was shown optimal for the NOON state [45–47] and a few other specific states [17, 43, 44, 48–50]. A similar situation happens for number counting [51–55], except that Hofmann found a class of path-symmetric states (PSSs) which, independent of the specific phase shift, allows the CR bound to be achieved [56]. However, the PSSs were only defined for pure states in conventional SU(2) interferometers [57]. While schemes widely used are variants of the SU(2) interferometry, the states are mixed states induced by the inevitable noises.

In this paper, we identify a large class of states which, regardless of the encoded phase, achieves the CR bound under the compound of parity and particle number measurements. These states cover all PSSs and some non-PSS ones. More remarkably, they can be generalized to include the mixed states, which is more relevant to experimental preparations of the input states. We propose a complete quantum phase estimation protocol with an arbitrary input state. The precision achieved through this protocol is always higher than or equal to that obtained via the original input state. We also demonstrate the implementation of the proposed OM scheme using a nonlinear interferometer and show the realization of the parity measurement in atomic condensates.

2. Pure state case

In the standard quantum metrology process [4], parameter θ is encoded into the phase of a quantum state $|\psi_{\rm in}\rangle$ through a unitary transformation

$$|\psi(\theta)\rangle = \mathrm{e}^{-\mathrm{i}\theta\hat{G}}|\psi_{\rm in}\rangle, \tag{1}$$

where the phase-shift generator $\hat{G}$ is a Hermitian operator. The eigenvalue and the corresponding eigenvector of $\hat{G}$ are denoted, respectively, as g_m and $|m\rangle$. Furthermore, we assume that the eigenvalues satisfy $g_m = -g_{-m}$, a condition fulfilled by SU(2) interferometry [57] and its widely used variants [14, 19, 58–61]. For convenience, we introduce the index $n \equiv |m|$. The phase-shift generator can be decomposed into

$$\hat{G} = \sum_{n>0} g_n \left(|\uparrow\rangle_{nn}\langle\uparrow| - |\downarrow\rangle_{nn}\langle\downarrow|\right), \tag{2}$$

where $|\uparrow\rangle_n \equiv |n\rangle$ and $|\downarrow\rangle_n \equiv |-n\rangle$. The possible $|n=0\rangle$ term has been dropped in equation (2) due to $g_0 = 0$ based on our assumption. Moreover, as shall become clear below, this term does not contribute to the QFI and is irrelevant to the discussion about OM. Therefore, we shall always assume that $n>0$ in all summations over n. We note that the phase-shift operator defined by equation (2) also covers the nonlinear generators $\hat{S}_z^3$ [62] and the Ising type Hamiltonian [63–66]. Additionally, for those multi-particle cases, $\hat{G}$ usually acts on the whole system concerned, leading $|\uparrow\rangle_n$ ($|\downarrow\rangle_n$) to illustrate a state of multiple particles instead of a single one. Now, independent of the measurement operator, the precision of θ's estimator is bounded by the CR inequality [1, 2]

$$\delta^2\theta \geqslant \frac{1}{\nu F\left(|\psi(\theta)\rangle, \hat{G}\right)}, \tag{3}$$

where ν is the repetitions of the measurement, and $F(|\psi(\theta)\rangle, \hat{G}) = 4\langle\psi_{\rm in}|\hat{G}^2|\psi_{\rm in}\rangle - 4\langle\psi_{\rm in}|\hat{G}|\psi_{\rm in}\rangle^2$ is the QFI that measures the variance of $\hat{G}$ with respect to $|\psi(\theta)\rangle$. Clearly, achieving higher precision for the estimation of θ relies not only on the initial state, which can lead to larger $F(|\psi(\theta)\rangle, \hat{G})$, but also on the measurement and estimation scheme, which allows the CR lower bound to be attained [1, 2, 39, 40]. Below, by explicitly constructing a set of measurement operators and the corresponding estimators, we show that an OM scheme exists for a large class of input states.

To this end, we partition the Hilbert space into a set of qubits, with the nth 'qubit' being defined by two basis states as $\mathcal{H}_n = \mathrm{span}\{|\uparrow\rangle_n, |\downarrow\rangle_n\}$, where n labels the qubit, and the range of n is determined by the spectrum of $\hat{G}^2$. We mention that: (i) the qubit $\mathcal{H}_n$ illustrates states of the whole system concerned instead of a single two-level particle; (ii) the whole Hilbert space is composed by the *direct sum*, instead of the direct product, of these qubits. Thus, a general input state can be expanded as the superposition of qubit states, i.e.,

$$|\psi_{\rm in}\rangle = \sum_n \sqrt{p_n}\mathrm{e}^{\mathrm{i}\varphi_n}|\alpha_n, \beta_n\rangle_n, \tag{4}$$

where $|\alpha_n, \beta_n\rangle_n = \cos\frac{\alpha_n}{2}\mathrm{e}^{-\mathrm{i}\beta_n/2}|\uparrow\rangle_n + \sin\frac{\alpha_n}{2}\mathrm{e}^{\mathrm{i}\beta_n/2}|\downarrow\rangle_n$ is the wave function of the nth qubit and $\sqrt{p_n}\mathrm{e}^{\mathrm{i}\varphi_n}$ is the probability amplitude with p_n (subjected to the constraint $\sum_n p_n = 1$) being the probability and φ_n being the phase.

The QFI of $|\psi(\theta)\rangle$ can be analytically evaluated to be

$$F\left(|\psi(\theta)\rangle, \hat{G}\right) = 4\sum_n p_n g_n^2 - 4\left(\sum_n p_n g_n \cos\alpha_n\right)^2, \tag{5}$$

where the first and second terms originate from $\langle\psi_{\rm in}|\hat{G}^2|\psi_{\rm in}\rangle$ and $\langle\psi_{\rm in}|\hat{G}|\psi_{\rm in}\rangle^2$, respectively. For a given set of $\{p_n\}$, a sufficient condition to maximize the QFI is $\alpha_n = \pi/2$, under which each qubit lies on the equator of its own Bloch sphere. The resulting input state,

$$|\psi_{\rm E}\rangle = \sum_n \sqrt{p_n}\mathrm{e}^{\mathrm{i}\varphi_n}|\frac{\pi}{2}, \beta_n\rangle_n, \tag{6}$$

is a superposition of equatorial qubits and is referred to as *equatorial state* (ES). As a comparison, the PSSs require that the global phase of the qubit φ_n is independent of n [56]. Therefore, $|\psi_{\mathrm{E}}\rangle$ covers not only all PSSs [56] but also the non-path-symmetric ones, such as the entangled coherent states [9, 10] and the one-axis twisting spin-squeezed states [12–14], as shown in appendix A. More importantly, as shall be shown, the ESs can also be generalized to the mixed state case.

To construct a projective measurement, we introduce a parity operator

$$\mathcal{P}_{\mathbf{0}} = \sum_n \left(|\downarrow\rangle_{nn}\langle\uparrow| + |\uparrow\rangle_{nn}\langle\downarrow|\right). \tag{7}$$

It can be easily verified that $\mathcal{P}_{\mathbf{0}}^2 = 1$ and the eigenvalues of $\mathcal{P}_{\mathbf{0}}$ are $p = \pm 1$. Physically, $\mathcal{P}_{\mathbf{0}}$ inverts the spectrum of $\hat{G}$ as $\mathcal{P}_{\mathbf{0}}\hat{G}\mathcal{P}_{\mathbf{0}} = -\hat{G}$. Next, we introduce a new set of basis states for the nth qubit as $|\mathbf{x}^{(+)}\rangle_n \equiv |\pi/2, 0\rangle_n$ and $|\mathbf{x}^{(-)}\rangle_n \equiv |\pi/2, \pi\rangle_n$, which are of even ($p = 1$) and odd ($p = -1$) parities, respectively. We then define the projection operators

$$\Pi_n^{(p)} = |\mathbf{x}^{(p)}\rangle_{nn}\langle\mathbf{x}^{(p)}|, \tag{8}$$

satisfying $\Pi_n^{(p)}\Pi_{n'}^{(p')} = \delta_{nn'}\delta_{pp'}\Pi_n^{(p)}$ and $\sum_{p=\pm}\sum_n \Pi_n^{(p)} = \mathbb{1}$. Apparently, $\{\Pi_n^{(p)}\}$ represents the compound measurements of $\mathcal{P}_{\mathbf{0}}$ and $\hat{G}^2$, i.e. $\{\Pi^{(\pm)}\}$ with $\Pi^{(\pm)} = \sum_n \Pi_n^{(\pm)}$ and $\{\Pi_n\}$ with $\Pi_n = \sum_{p=\pm}\Pi_n^{(p)}$. In fact, they can be measured both simultaneously and sequentially since $[\mathcal{P}_{\mathbf{0}}, \hat{G}^2] = 0$.

Now, let us perform the measurement on an ensemble of the identical states $e^{-i\theta\hat{G}}|\psi_{\mathrm{E}}\rangle$ and denote the number of the outcomes corresponding to $\Pi_n^{(p)}$ after total ν repeated measurements as $\nu_n^{(p)}$. The construction of the optimal estimator can be proceeded as follows. For each set of the binary outcomes corresponding to $\{\Pi_n^{(+)}, \Pi_n^{(-)}\}$, we construct an unbiased estimator Θ_n based on the maximum likelihood estimation. The variance of Θ_n is $\delta^2\Theta_n = 1/(\nu_n F_n)$ with $\nu_n = \nu_n^{(+)} + \nu_n^{(-)}$ and $F_n = 4g_n^2$ [67]. When repetition $\nu \to \infty$, we have $\delta^2\Theta_n \to 1/(\nu p_n F_n)$. Then, we choose the total estimator as the linear combination of all single-qubit estimators, i.e.

$$\Theta = \sum_n w_n \Theta_n, \tag{9}$$

where the weights w_n satisfy $w_n \geqslant 0$ and $\sum_n w_n = 1$. Apparently, Θ is still unbiased and its variance is $\delta^2\Theta = \sum_n w_n^2 \delta^2\Theta_n$. It can be further shown that $\delta^2\Theta$ is minimized if $w_n = p_n F_n / F$, where $F = \sum_n p_n F_n$ is the QFI of $\mathrm{e}^{-\mathrm{i}\theta\hat{G}}|\psi_{\mathrm{E}}\rangle$. The minimal variance,

$$\left(\delta^2\Theta\right)_{\min} = \frac{1}{\nu F}, \tag{10}$$

is exactly the CR lower bound, which proves that $\{\Pi_n^{(p)}\}$ indeed represents an OM.

We comment that the optimal measurability achieved in the above scheme can be attributed to the following reasons: (i) For ESs, the QFI of the individual qubit is maximized and the parity measurement is optimal; (ii) The contributions to the total QFI from distinct qubits are decoupled (see equation (5)) such that we may perform the OM on individual qubits and construct estimator separately; (iii) The weight w_n in the total estimator in equation (9) is inversely proportional to $\delta^2\Theta_n$, which warrants the efficient usage of all resources.

3. Mixed state case

The pure state results can be generalized to the mixed state case straightforwardly. In order to find the desired density matrix ρ_{E} for the input state, we recall that one of the reasons the proposed scheme works for pure states is that every qubit is an ES. Therefore, the minimum requirement for ρ_{E} is that one should obtain an equatorial qubit when projected to an arbitrary qubit subspace, i.e.

$$\Pi_n \rho_{\mathrm{E}} \Pi_n \propto \left|\frac{\pi}{2}, \beta_n\right\rangle_{nn}\left\langle\frac{\pi}{2}, \beta_n\right| \tag{11}$$

for any $\Pi_n = \Pi_n^{(+)} + \Pi_n^{(-)}$. Correspondingly, the explicit form of the density matrix is

$$\rho_{\mathrm{E}} = \sum_n p_n \left|\frac{\pi}{2}, \beta_n\right\rangle_{nn}\left\langle\frac{\pi}{2}, \beta_n\right| + \sum_{m\neq n}\left(\gamma_{mn}\left|\frac{\pi}{2}, \beta_m\right\rangle_{mn}\left\langle\frac{\pi}{2}, \beta_n\right| + \mathrm{h.c.}\right), \tag{12}$$

where $|\gamma_{mn}|^2 \leqslant p_n p_m$ due to the decoherence. This equation merely states that $\rho_{\rm E}$ is supported by a *unique* ES of each qubit subspace.

To see that the OM can be attained with $\rho_{\rm E}$, we evaluate the QFI of the parametrized state $\rho(\theta) = {\rm e}^{-{\rm i}\theta\hat{G}}\rho_{\rm E}{\rm e}^{{\rm i}\theta\hat{G}}$, i.e. $F\big(\rho(\theta),\hat{G}\big) = {\rm tr}(\rho(\theta)L^2)$, where L is the symmetric logarithmic derivative of ρ that satisfies $\partial_\theta\rho(\theta) = \frac{1}{2}(L\rho+\rho L)$ and $L^\dagger = L$ [2]. It can be directly verified that, in the $\hat{G}$ representation,

$$L = 2{\rm i}\sum_n g_n\left[{\rm e}^{{\rm i}(2g_n\theta+\beta_n)}|\downarrow\rangle_{nn}\langle\uparrow| - {\rm h.c.}\right] \tag{13}$$

fulfills our purpose. Straightforward calculations give rise to $F\big(\rho_{\rm E},\hat{G}\big) = 4\sum_n p_n g_n^2$, which is again the sum of QFI of individual qubit. Now, by applying the measurement $\{\Pi_n^{(p)}\}$ and constructing the same estimators $\{\Theta_n\}$ and Θ as in the pure-state case, we can also attain the minimum variance of Θ (equation (10)), which confirms the optimality of the compound measurements for mixed state $\rho_{\rm E}$.

We note that $\rho_{\rm E}$ may be treated as the mixed state decohered from the pure state $|\psi_{\rm E}\rangle$. The fact that these two states have equal QFI given the same set of $\{p_n\}$ indicates that not all quantum coherence is usable for improving the precision of phase estimation. This can also be seen from the symmetric logarithmic derivative, equation (13), in which γ_{mn} is completely absent. Additionally, in the construction of Θ, all estimators Θ_n and weights w_n are independent of γ_{mn}, which implies that the coherence between distinct qubits is irrelevant to the phase estimation.

Since the system-bath couplings that induce the decoherence are unavoidable, it is interesting to find the condition under which the optimal measurability of the input state, $|\psi_{\rm E}\rangle$ or $\rho_{\rm E}$, is maintained. To this end, we formally express the overall Hamiltonian (system plus bath) as

$$H = \sum_\kappa H_\kappa \otimes B_\kappa, \tag{14}$$

where H_κ and B_κ are operators defined on the Hilbert spaces for system and bath, respectively, and B_κ are linearly independent [68]. We then define a generalized state-dependent parity operator

$$\mathcal{P}_{\boldsymbol\beta} = \sum_n\left({\rm e}^{{\rm i}\beta_n}|\downarrow\rangle_{nn}\langle\uparrow| + {\rm e}^{-{\rm i}\beta_n}|\uparrow\rangle_{nn}\langle\downarrow|\right), \tag{15}$$

where β_n are given by the state $|\psi_{\rm E}\rangle$ or $\rho_{\rm E}$. It can be shown that a sufficient condition for equation (11) being satisfied by the density matrix of the system is

$$[H_\kappa,\mathcal{P}_{\boldsymbol\beta}] = 0 \text{ for any } \kappa. \tag{16}$$

Remarkably, even if this condition is not satisfied, the optimal measurability can still be approximately preserved through dynamical decoupling [68, 69]. In fact, by noting that $\mathcal{P}_{\boldsymbol\beta}$ is a unitary operator, we introduce the so-called $\mathcal{P}_{\boldsymbol\beta}$ pulse, which transforms a state of the system according to $\rho\to\mathcal{P}_{\boldsymbol\beta}\rho\mathcal{P}_{\boldsymbol\beta}$. Then, by applying a sequence of $\mathcal{P}_{\boldsymbol\beta}$ pulses with a sufficiently small inter-pulse interval, the time evolution of the system and bath is driven by the effective overall Hamiltonian $\bar{H} = \sum_\kappa \bar{H}_\kappa\otimes B_\kappa$, where $\bar{H}_\kappa = \frac{1}{2}\left[H_\kappa + \mathcal{P}_{\boldsymbol\beta}H_\kappa\mathcal{P}_{\boldsymbol\beta}\right]$. Clearly, the optimal measurability is maintained since $[\bar{H}_k,\mathcal{P}_{\boldsymbol\beta}] = 0$ for any κ. We comment that the possible scenarios for applying dynamical decoupling include the input state preparation and the state storage, for which the system is very likely exposed to the environment.

4. Parity-enhanced phase-estimation scheme

In addition to being used for measurement and estimation, parity measurement also increases the QFI of the input state. To see this, we consider a general state ρ whose QFI satisfies the inequality $F(\rho,\hat{G}) \leqslant 4{\rm tr}(\rho\hat{G}^2) - 4{\rm tr}(\rho\hat{G})^2$. After performing the parity measurement $\mathcal{P}_{\mathbf{0}}$ on ρ, the state collapses into the ESs

$$\rho^{(\pm)} = \Pi^{(\pm)}\rho\Pi^{(\pm)}/q^{(\pm)}, \tag{17}$$

where $\Pi^{(\pm)} = \sum_n \Pi_n^{(\pm)}$ are projections to the even- and odd-parity subspaces, respectively, and $q^{(\pm)} = {\rm tr}(\rho\Pi^{(\pm)})$ are the probabilities to obtain the outcomes ±1. The average QFI of the resulting states is

$$\bar{F} = \sum_{p=\pm} q^{(p)}F\left(\rho^{(p)},\hat{G}\right) = 4{\rm tr}\left(\rho\hat{G}^2\right) \geqslant F\left(\rho,\hat{G}\right), \tag{18}$$

which indicates that the measuring $\mathcal{P}_{\mathbf{0}}$ indeed improves the quality of the input state.

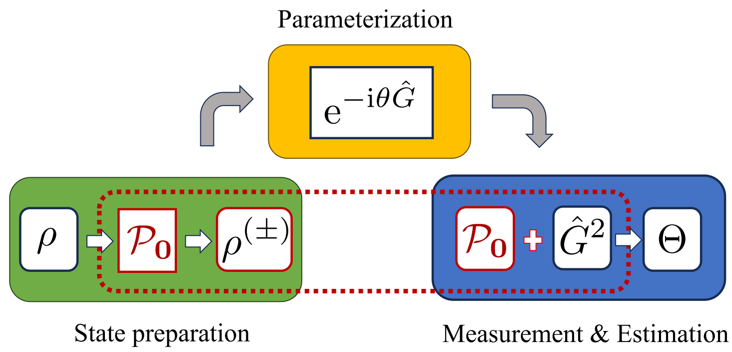

Figure 1. Schematics for the protocol of optimal phase estimation. (i) An ES can be prepared directly or via a parity measurement $\mathcal{P}_\mathbf{0}$. (ii) A phase θ is encoded by the generator $\hat{G}$. (iii) CR bound of the phase estimation precision is attained with the compound measurements $\mathcal{P}_\mathbf{0}$ and $\hat{G}^2$ and with the estimator Θ.

In figure 1, we schematically summarize the protocol for optimal phase estimation. Interestingly, for state preparation, if the input state is an eigenstate of $\hat{G}$, say $|\uparrow\rangle_n$, a parity measurement would yield an ES, $|\mathbf{x}^{(\pm)}\rangle_n$, in the nth qubit subspace. Correspondingly, the QFI of the input state is increased from zero to $4g_n^2$. In particular, the QFI is maximized if g_n^2 is the largest eigenvalue of $\hat{G}^2$. Therefore, the efficiency of parity measurement for input state preparation can be extremely high. It is worth mentioning that, besides being used for state preparation and measurement, parity is also useful for state storage as discussed in section 3.

5. Nonlinear

To demonstrate the applications of the proposed scheme, we consider a nonlinear interferometer modeled by the Hamiltonian

$$H_{\mathrm{NI}}(t) = -\chi\hat{S}_z^2 - B_x(t)\hat{S}_x - B_z\hat{S}_z, \tag{19}$$

where, for a two-mode system, say modes a and b, the angular momentum operators are defined as $\hat{S}_x = (\hat{a}^\dagger\hat{b} + \hat{b}^\dagger\hat{a})/2$, $\hat{S}_y = (\hat{a}^\dagger\hat{b} - \hat{b}^\dagger\hat{a})/(2\mathrm{i})$, and $\hat{S}_z = (\hat{a}^\dagger\hat{a} - \hat{b}^\dagger\hat{b})/2$ with $\hat{a}$ and $\hat{b}$ being the annihilation operators for modes a and b, respectively, and $\hat{S}_z$ is the phase generator. Furthermore, χ (>0) is the nonlinear coupling strength, B_x and B_z are transverse and longitudinal fields, respectively. We point out that Hamiltonian (19) can be realized by either external or internal states of N Bose condensed atoms [19, 58–61]. In the following discussions, we take N even without losing the generality. Considering $\hat{G}(=\hat{S}_z)$ is a collective spin operator, the qubit $\mathcal{H}_n$ illustrates states of all N atoms with $|\uparrow\rangle_n(|\downarrow\rangle_n) = |m_z = \pm n\rangle_z$.

To start, let us first briefly recall the eigen-spectrum of H_{NI} in the absence of the longitudinal field B_z [58, 61], says H_{Pre}, as shown in figure 2(a). For $B_x \gg N\chi$, the eigenstates of H_{Pre} are those of $\hat{S}_x$, i.e. $|m_x = m\rangle_x$ with $m = -N/2, -N/2+1, \ldots, N/2$. In particular, the parity of $|m_x\rangle_x$ with respect to $\mathcal{P}_0$ is $(-1)^{N/2-m_x}$. Actually, the kth excited state of H_{Pre} has a certain parity $(-1)^k$ for arbitrary $B_x \neq 0$, with $k = 1, 2, \ldots, N$, and $k = 0$ denoting the ground state. While at the $B_x = 0$, the eigenstates of H_{Pre} are those of $\hat{S}_z^2$ which are doubly degenerate. By varying B_x, the two sets of spectra with $B_x \gg N\chi$ and $B_x = 0$ are adiabatically connected according to

$$|\mathbf{x}^{(\pm)}\rangle_n \leftrightarrow |m_x = 2n - (N+1\mp1)/2\rangle_x, \tag{20}$$

with $|\mathbf{x}^{(+)}\rangle_0 = |m_z = 0\rangle_z$ additionally. The nonlinear interferometry is generally operated as follows. Initially, the system is prepared in state $|\Psi_0\rangle = |m_x = N/2\rangle_x$ under a large B_x. The transverse field is then swept to zero, which gives rise to the input state for the interferometry $|\Psi_{\mathrm{in}}\rangle = \sum_n c_n|\mathbf{x}^{(+)}\rangle_n$, where c_n depend on the sweeping rate $v = -\mathrm{d}B_x/\mathrm{d}t$. Clearly, $|\Psi_{\mathrm{in}}\rangle$ is an ES with all $\beta_n = 0$, as exemplified in figure 2. We remark that $|\Psi_{\mathrm{in}}\rangle$ has the same even parity as that of $|\Psi_0\rangle$ since the Hamiltonian H_{Pre} for input preparation converses $\mathcal{P}_\mathbf{0}$. Furthermore, as discussed in section 3, even in the presence of stray fields, the parity conservation can be recovered via dynamical decoupling with $\mathcal{P}_\mathbf{0} = (-1)^{N/2}\mathrm{e}^{-\mathrm{i}\pi\hat{S}_x}$ pulse.

To proceed further, we turn on the longitudinal field for a time interval Δt, which encodes the phase $\theta = -B_z\Delta t$ into the wave function through $|\Psi(\theta)\rangle = \mathrm{e}^{-\mathrm{i}\Delta t H_{\mathrm{NI}}}|\Psi_{\mathrm{in}}\rangle$ with $B_x = 0$. We remark that $|\Psi(\theta)\rangle$ is still an ES since the nonlinear term $\hat{S}_z^2$ only contributes a global phase, $\mathrm{e}^{-\mathrm{i}\Delta t\chi\hat{S}_z^2}$, to each qubit. However, it is not a PSS due to this phase by following the discussions below equation (6). Finally, we adiabatically increase

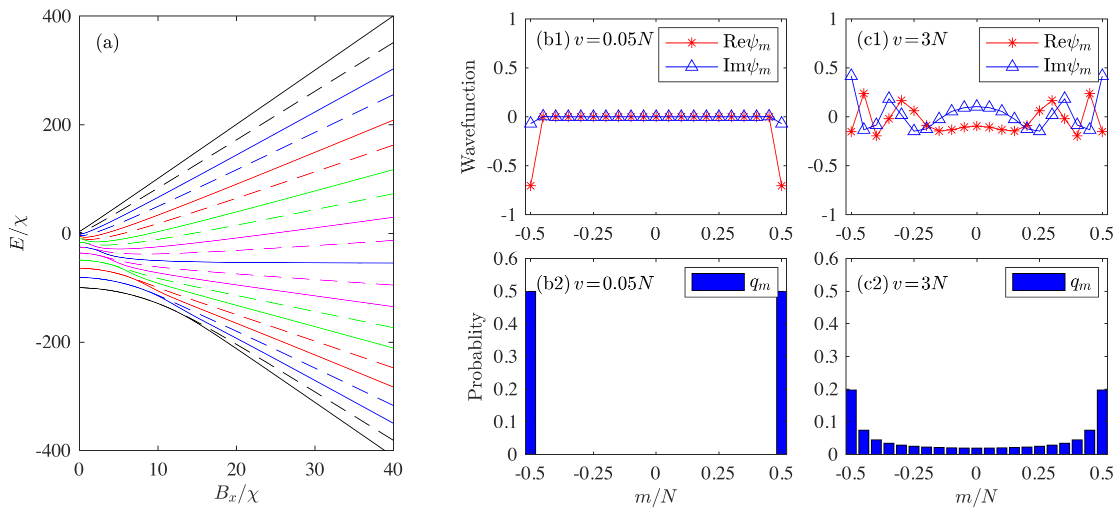

Figure 2. Preparing equatorial states with the nonlinear interferometer. (a) Eigen-spectrum of the Hamiltonian $H_{\mathrm{NI}}(t)$ with $N = 20$, $B_z = 0$. Solid (dashed) lines denote eigenstates with even (odd) parity with respect to $\mathcal{P}_0$. An equatorial state $|\Psi_{\mathrm{in}}\rangle$ is prepared via sweeping B_x. (b1)–(c2) Wave function and probability distribution of the state prepared. We set $\psi_m = {}_z\langle m_z = m|\Psi_{\mathrm{in}}\rangle$, $q_m = |\psi_m|^2$, $B_x = B_0 - vt$, with $B_0 = 2.5N$, $v = 0.05N$ and $3N$, respectively. The symmetry $q_m = q_{-m}(= p_{|m|}/2$ if $m \neq 0)$ indicates that $|\Psi_{\mathrm{in}}\rangle$ is an equatorial state. The symmetry $\psi_m = \psi_{-m}$ indicates that $|\Psi_{\mathrm{in}}\rangle$ is even parity with all $\beta_n = 0$. Specifically, (b1) and (b2) indicate the $|\Psi_{\mathrm{in}}\rangle$ prepared via $v = 0.05N$ (almost) a multi-partite GHZ state.

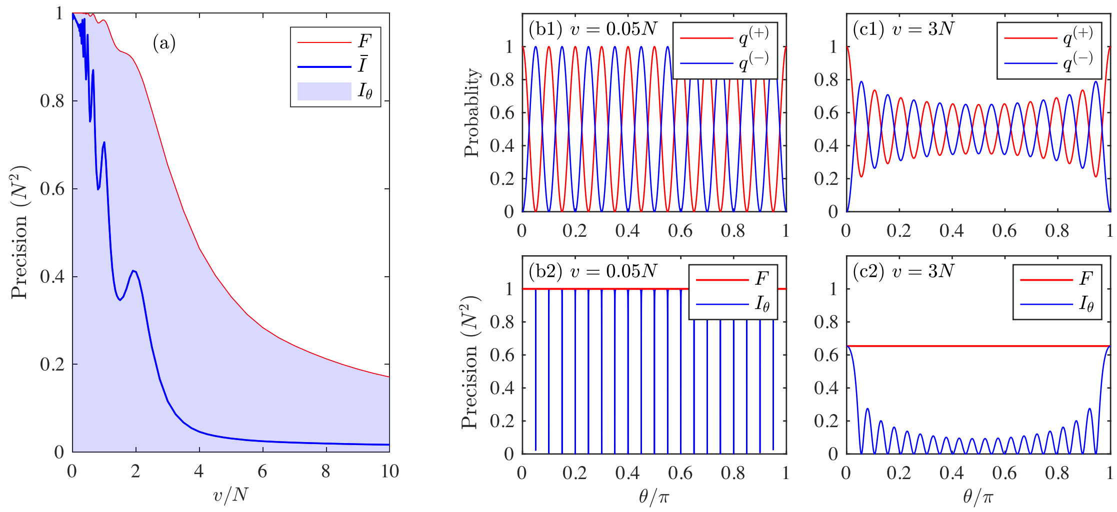

Figure 3. Precision of the nonlinear interferometer ($N = 20$) (a) Precision (Fisher information) as the function of sweeping rate, where we set $B_x = B_0 - vt$, with $B_0 = 2.5N$. The QFI F measures the precision acquired via the proposed measurement. I_θ denotes the precision acquired via solely the parity measurement. $\bar{I}$ denotes average of I_θ over $\theta \in [0, 2\pi)$. (b1)–(c2) Probability and precision acquired via implementing solely the parity measurement under the sweeping rate $v = 0.05N$ and $3N$, respectively.

B_x to a value much larger than $N\chi$, which maps $|\mathbf{x}^{(\pm)}\rangle_n$ back to the eigenstate of $\hat{S}_x$ based on equation (20). The measurement $\{\Pi_n^{(\pm)}\}$ can then be realized by measuring $\hat{S}_x$ with the resulting state.

We point out that $\{\Pi_n^{(\pm)}\}$ is intrinsically a collective measurement of all N condensed atoms. Its realization relies on two conditions: (i) the energy spectrum of H_{NI} is nondegenerate, which is generally true unless there exist accidental degeneracies; (ii) $\hat{S}_x$ is directly measurable by, e.g. the Stern–Gerlach apparatus. Otherwise, one can also apply more sophisticated approaches, such as the scheme proposed in [58], or the compound measurement will be discussed in section 6.

Next, we show the performance of the proposed scheme in figures 2 and 3, where its precision is characterized via the QFI $F(|\Psi(\theta)\rangle, \hat{S}_z)$ for its optimality. When sweeping the transverse field almost adiabatically (e.g. $v = 0.05N$), the prepared input state $|\Psi_{\mathrm{in}}\rangle$ is almost a NOON state, and the precision is at the Heisenberg level. The precision is decreased at a large sweeping rate, e.g. $v = 3N$. It is induced by the redistribution of probability over the qubits, as shown by $p_n(= q_n + q_{-n})$ in figure 2(c2).

We mention that optimality of the proposed measurement scheme is independent of the encoded phase θ and the sweeping rate v. It is priory to implement solely the parity measurement $\mathcal{P}_0$, i.e. $\{\Pi^{(\pm)}\}$ on $|\Psi(\theta)\rangle$

under large sweeping speed v, as shown in figure 3. Specifically, we quantify the precision of solely parity measurement with the classical Fisher information $I_\theta = \sum_{p=\pm}(\partial_\theta q^{(p)})^2/q^{(p)}$ correspondingly, with $q^{(\pm)} = \langle\Psi(\theta)|\Pi^{(\pm)}|\Psi(\theta)\rangle$. As shown by figure 3(b2), the solely parity measurement is almost optimal ($I_\theta \approx F$) for all θ when $|\Psi_{\rm in}\rangle$ is prepared almost adiabatically. However, for states $|\Psi_{\rm in}\rangle$ prepared with large v, I_θ highly depends on the parameter θ and is only optimal with $\theta \to k\pi$. The average precision $\bar{I} := \frac{1}{2\pi}\int_0^{2\pi} d\theta I_\theta$ is thus drastically decreased with the increase of v.

Additionally, we emphasize that the transverse field B_x is not necessarily swept linearly in the state preparation process, for the critical points are: (i) the conservation of parity, which guarantees the prepared input state is an ES; (ii) $\chi > 0$, which leads the qubits with larger QFI (eigenvalue g_n^2) has larger population probability. Recently, a machine optimization method has been applied in [70] to manipulate the transverse field in a state preparation Hamiltonian similar to $H_{\rm Pre}$. The input state they prepared, named the spin cat state, is also an ES resulting from conserving $\mathcal{P}_{\mathbf{0}}$ equivalently.

6. Realization of non-demolition parity measurement

Suppose $\{\Pi_n^{(\pm)}\}$ cannot be implemented as a single measurement. In that case, one may measure $\mathcal{P}_{\mathbf{0}}$ and $\hat{G}^2$ sequentially, which requires that the measurement of $\mathcal{P}_{\mathbf{0}}$ is non-demolition as those experimentally realized in various systems [71–75]. Here, as an example, we demonstrate its realization in a two-mode atomic system, for which the parity operator becomes

$$\mathcal{P}_{\mathbf{0}} = (-1)^{S-\hat{S}_x} = \mathrm{e}^{-\mathrm{i}\pi\hat{S}_y/2}(-1)^{\hat{b}^\dagger\hat{b}}\mathrm{e}^{\mathrm{i}\pi\hat{S}_y/2}. \tag{21}$$

As can be seen, other than the $\pi/2$ rotations around the y-axis, the measurement of $\mathcal{P}_{\mathbf{0}}$ is reduced to that of $(-1)^{\hat{b}^\dagger\hat{b}}$ which, in analogue to the parity measurement of the photon number in a cavity [72], can be realized by introducing an ancilla qubit coupling to mode $\hat{b}$ of the system. Specifically, we assume the qubit-system coupling Hamiltonian takes the form

$$H_{\rm qs}/\hbar = \omega_{\rm q}|e\rangle\langle e| + \chi_{\rm qs}\hat{b}^\dagger\hat{b}|e\rangle\langle e|, \tag{22}$$

where $\hbar\omega_{\rm q}$ is the energy difference between the ground state, $|g\rangle$, and the excited state, $|e\rangle$, of the qubit, and $\chi_{\rm qs}$ is the qubit-system coupling strength. In appendix B, we show how to engineer Hamiltonian equation (22) with the internal states of atoms. In the rotating frame of the qubit, the excited state of the qubit acquires a phase $\Phi = \chi_{\rm qs}\hat{b}^\dagger\hat{b}t$ proportional to the atom number in mode $\hat{b}$. By carefully choosing the evolution time t such that $\chi_{\rm qs}t = \pi$, we realize the operation $U_\pi = (-1)^{\hat{b}^\dagger\hat{b}} \otimes |e\rangle\langle e| + \hat{I}_{\rm s} \otimes |g\rangle\langle g|$, where $\hat{I}_{\rm s}$ is the identity operator of the system. Then, by inserting U_π between $\pi/2$ and $-\pi/2$ rotations around the y axis for both qubit and system, we realize a controlled-X gate

$$\begin{aligned} C_X &= \left[\mathrm{e}^{-\mathrm{i}\pi\hat{S}_y/2} \otimes R_y^\dagger\left(\tfrac{\pi}{2}\right)\right] U_\pi \left[\mathrm{e}^{\mathrm{i}\pi\hat{S}_y/2} \otimes R_y\left(\tfrac{\pi}{2}\right)\right] \\ &= \Pi^{(+)} \otimes \hat{I}_{\rm q} + \Pi^{(-)} \otimes \hat{\sigma}_x, \end{aligned} \tag{23}$$

where $R_y(\pi/2)$ is the $\pi/2$ rotation of the qubit around the y-axis, $\hat{I}_{\rm q}$ is the identity operator of the qubit, and $\hat{\sigma}_x = \big(|e\rangle\langle g| + |g\rangle\langle e|\big)$ flips the qubit. To perform the measurement, we may prepare the qubit in $|g\rangle$ state initially, C_X then couples the even (odd) parity state of the system to $|g\rangle$ ($|e\rangle$). A subsequent projective measurement $\{|g\rangle\langle g|, |e\rangle\langle e|\}$ on the qubit will leave the system in a parity-definite state, which completes the measurement $\{\Pi^{(+)}, \Pi^{(-)}\}$, i.e. $\mathcal{P}_{\mathbf{0}}$ on the system.

Additionally, measuring $\hat{G}^2$ indicates a set of projectors $\{\Pi_n\}$. However, if the non-demolition parity measurement has been performed, one can measure the operator $\hat{G} = \hat{S}_z$, i.e. $\{|m_z\rangle_{zz}\langle m_z|\}$ instead. It can be realized by counting the particle number difference between mode $\hat{a}$ and $\hat{b}$.

7. Conclusions

We have proposed an OM scheme for the pure and mixed ESs, which cover a wide range of the input states in various interferometry. Based on the compound measurement of parity and particle number, the scheme allows us to unveil more information about the states than the single measurement of either one. We have also proposed a protocol for phase estimation by including the state preparation using parity measurement, in which the precision achieved consistently surpasses that of the standard protocol. We also demonstrate the implementation of the proposed OM scheme using nonlinear interferometry and show the realization of the parity measurement in atomic condensates.

Data availability statement

All data that support the findings of this study are included within the article (and any supplementary files).

Acknowledgments

H J X thanks Yingdan Wang and Stefano Chesi for the helpful discussion. This work was supported by the NSFC (Grant Nos. 12135018, 12088101, and U2330401), NKRDPC (Grant No. 2021YFA0718304), and the Fundamental Research Funds for the Central Universities (Grant No. 2412023QD007).

Appendix A. Examples of equatorial states

A.1. Path-symmetric states

Hofmann formalizes the PSSs in the conventional SU(2) interferometry, where the phase generator reads $\hat{G} = \hat{S}_z$ [56]. In $\hat{S}_z$'s representation, the PSS is defined as a state $|\psi\rangle$ satisfying ${}_z\langle m_z|\psi\rangle = {}_z\langle -m_z|\psi\rangle^* \mathrm{e}^{-2\mathrm{i}\chi_0}$ for all of the eigenstates $|m_z\rangle_z$ of $\hat{S}_z$. It is equivalent to letting $\alpha_n = \frac{\pi}{2}$, $\varphi_n = -\chi_0$ up to $k_n\pi$, for all $n > 0$ (and $n = 0$ if $|0\rangle$ exists) in equation (4), with $k_n \in \mathbb{Z}$. We mention that the ES is defined in equation (6) via constraining $\alpha_n = \frac{\pi}{2}$ for all $n > 0$. It indicates that the PSS is a particular subclass of the ES with additional constraints on $\{\varphi_n\}$. Exemplified by the system with even particle number N, we have the PSS

$$\begin{aligned}|\mathrm{PSS}\rangle_\theta &= \mathrm{e}^{-\mathrm{i}\hat{G}\theta}\left[\sum_{n>0}(-1)^{k_n}\sqrt{p_n}\mathrm{e}^{-\mathrm{i}\chi_0}\frac{1}{\sqrt{2}}\left(\mathrm{e}^{-\mathrm{i}\beta_n/2}|n\rangle + \mathrm{e}^{\mathrm{i}\beta_n/2}|-n\rangle\right) + (-1)^{k_0}\sqrt{p_0}\mathrm{e}^{-\mathrm{i}\chi_0}|0\rangle\right]\\ &= \sum_{n>0}(-1)^{k_n}\sqrt{p_n}\mathrm{e}^{-\mathrm{i}\chi_0}\frac{1}{\sqrt{2}}\left(\mathrm{e}^{-\mathrm{i}(g_n\theta+\beta_n/2)}|n\rangle + \mathrm{e}^{\mathrm{i}(g_n\theta+\beta_n/2)}|-n\rangle\right)\\ &\quad + (-1)^{k_0}\sqrt{p_0}\mathrm{e}^{-\mathrm{i}\chi_0}|0\rangle, \end{aligned} \tag{A.1}$$

and the qubit $\mathcal{H}_n = \mathrm{span}\{|n\rangle, |-n\rangle\}$, where $|\pm n\rangle = |m_z = \pm n\rangle_z$ with $g_{\pm n} = \pm n$ and the additional state $|0\rangle = |m_z = 0\rangle_z$ with $g_0 = 0$.

A.2. Examples of equatorial states

In this subsection, we formalize four classes of widely used quantum states to the ESs form, which contains both the path-symmetric and non-PSSs. Without losing the generality, we set N even in the following examples.

(i) Spin coherent states (spin-$\frac{1}{2}$ system) with phase generator $\hat{G} = \sum_{l=1}^N \hat{S}_z^{(l)}$.

$$\begin{aligned}|\mathrm{SCS}\rangle_\theta &= \mathrm{e}^{-\mathrm{i}\hat{G}\theta}\otimes_{l=1}^N\tfrac{1}{\sqrt{2}}\left(\left|m_z^{(l)}=\tfrac{1}{2}\right\rangle_l + \left|m_z^{(l)}=-\tfrac{1}{2}\right\rangle_l\right)\\ &= \sum_{m=1}^{N/2}\frac{c_m}{\sqrt{2}}\left(\mathrm{e}^{-\mathrm{i}m\theta}\left|\tfrac{N}{2},m\right\rangle_z + \mathrm{e}^{\mathrm{i}m\theta}\left|\tfrac{N}{2},-m\right\rangle_z\right)\\ &\quad + \frac{c_0}{\sqrt{2}}\left|\tfrac{N}{2},0\right\rangle_z, \end{aligned} \tag{A.2}$$

with $c_m = 2^{-(N-1)/2}\binom{N}{N/2+m}^{1/2}$. The nth qubit $\mathcal{H}_n$ is defined as

$$\mathcal{H}_n = \mathrm{span}\left\{\left|\tfrac{N}{2},n\right\rangle_z, \left|\tfrac{N}{2},-n\right\rangle_z\right\}, \tag{A.3}$$

with probability $p_n = 2^{1-N}\binom{N}{N/2+n}$ for $n = 1,\ldots,\frac{N}{2}$, and $\mathcal{H}_0 = \{\left|\frac{N}{2},0\right\rangle_z\}$ with $p_0 = 2^{-N}\binom{N}{N/2}$. The QFI of $|\mathrm{SCS}\rangle_\theta$ is $F = 4\sum_n p_n n^2 = N$, which indicates the precision is still in the standard quantum limit. It is captured by figure A1(a), which shows that $\{p_n\}$ mainly distributes around qubits with small eigenvalues.

(ii) One-axies twisting spin squeezed states. We follow the definition in [13] and take the phase generator as $\hat{G} = \hat{a}^\dagger\hat{a} - N/2$. The squeezed state reads

$$
\begin{aligned}
|\mathrm{SS}\rangle_\theta &= \mathrm{e}^{-\mathrm{i}\theta\hat{G}}\hat{R}_x(-\nu)\,\mathrm{e}^{-\mathrm{i}\hat{H}_{SS}t}\hat{R}_y\left(\tfrac{\pi}{2}\right)|N\rangle_a|0\rangle_b \\
&= \sum_{m=0}^{N/2-1}\frac{c_m}{\sqrt{2}}\left(\mathrm{e}^{-\mathrm{i}\theta\left(m-\frac{N}{2}\right)}|m\rangle_a|N-m\rangle_b+\mathrm{e}^{\mathrm{i}\theta\left(m-\frac{N}{2}\right)}|N-m\rangle_a|m\rangle_b\right) \\
&\quad+\tfrac{c_{N/2}}{\sqrt{2}}\left|\tfrac{N}{2}\right\rangle_a\left|\tfrac{N}{2}\right\rangle_b,
\end{aligned} \tag{A.4}
$$

where the squeezing operator is $\hat{H}_{SS}=\chi\hat{S}_z^2$ with the squeezing parameter $\mu=2\chi t$, $c_m=\frac{1}{\sqrt{2^{N-1}}}\sum_{k,\omega}\binom{N}{k}\binom{k}{\omega}\binom{N-k}{m-\omega}\binom{N}{m}^{-1/2}e^{-\mathrm{i}h}(\cos[\frac{\nu}{2}])^{N-g}(\mathrm{i}\sin[\frac{\nu}{2}])^g$ with $g=k+m-2\omega$ and $h=\mu(N-2k)^2/8$. We mention that c_m generally carries a m-dependent phase. It makes $|\mathrm{SS}\rangle_\theta$ generally a non-PSS. The nth qubit is defined as

$$
\mathcal{H}_n=\mathrm{span}\left\{|\tfrac{N}{2}+n\rangle_a|\tfrac{N}{2}-n\rangle,|\tfrac{N}{2}-n\rangle_a|\tfrac{N}{2}+n\rangle_b\right\}, \tag{A.5}
$$

for $n=1,2,\ldots,\frac{N}{2}$. The phase θ is encoded as $\beta_n(\theta)=2n\theta$. The probability of $|\mathrm{SS}\rangle_\theta$ projected to $\mathcal{H}_n$ reads $p_n=2^{-\delta_{n,0}}c^2_{n+N/2}$. In figure A1(b), we illustrated p_n with $\mu=\pi/2$ and $\nu=\pi/2$.

(iii) Twin Fock states with state preparation $\hat{R}_y(\frac{\pi}{2})=\exp[\pi(\hat{b}^\dagger\hat{a}-\hat{a}^\dagger\hat{b})/4]$ and phase generator $\hat{G}=\hat{a}^\dagger\hat{a}-N$.

$$
\begin{aligned}
|\mathrm{TF}\rangle_\theta &= e^{-\mathrm{i}\theta\hat{G}}\hat{R}_y\left(\tfrac{\pi}{2}\right)|N\rangle_a|N\rangle_b \\
&= \sum_{k=0}^{N/2-1}\frac{c_k}{\sqrt{2}}\left(\mathrm{e}^{\mathrm{i}\theta(N-2k)}|2k\rangle_a|2N-2k\rangle_b+\mathrm{e}^{-\mathrm{i}\theta(N-2k)}|2N-2k\rangle_a|2k\rangle_b\right) \\
&\quad+\frac{c_{N/2}}{\sqrt{2}}|N\rangle_a|N\rangle_b,
\end{aligned} \tag{A.6}
$$

with $c_k=\frac{(-1)^k}{2^{N-1/2}}\left[\binom{2k}{k}\binom{2N-2k}{N-k}\right]^{1/2}$. The qubit is defined as

$$
\mathcal{H}_n=\mathrm{span}\left\{|N+n\rangle_a|N-n\rangle_b,|N-n\rangle_a|N+n\rangle_b\right\}, \tag{A.7}
$$

with the corresponding probability $p_n=[c_{(N-n)/2}]^2/2^{\delta_{n,0}}$ if n is even, and $p_n=0$ if n is odd. We plot the distribution p_n in figure A1(c). It shows that qubits with larger eigenvalues (g_n^2) are more likely to be occupied, such that the twin Fock states have larger QFI than $|\mathrm{SCS}\rangle_\theta$.

(iv) Entangled coherent states with phase generator $\hat{G}=\hat{a}^\dagger\hat{a}-\hat{b}^\dagger\hat{b}$.

$$
\begin{aligned}
|\mathrm{ECS}\rangle_\theta &= r^{-1/2}e^{-|\alpha|^2/2}\sum_{n=0}^{\infty}\frac{\alpha^n}{n!}\left[\hat{a}^{\dagger n}\mathrm{e}^{-\mathrm{i}n\theta}+\hat{b}^{\dagger n}\mathrm{e}^{\mathrm{i}n\theta}\right]|0\rangle_a|0\rangle_b \\
&= r^{-1/2}e^{-|\alpha|^2/2}\sum_{n=1}^{\infty}\frac{\alpha^n}{(n!)^{1/2}}\left(\mathrm{e}^{-\mathrm{i}n\theta}|n\rangle_a|0\rangle_b+e^{\mathrm{i}n\theta}|0\rangle_a|n\rangle_b\right) \\
&\quad+2r^{-1/2}e^{-|\alpha|^2/2}|0\rangle_a|0\rangle_b
\end{aligned} \tag{A.8}
$$

with $r=2(1+e^{-|\alpha|^2})$. The qubit is defined as

$$
\mathcal{H}_n=\mathrm{span}\left\{|n\rangle_a|0\rangle_b,|0\rangle_a|n\rangle_b\right\}, \tag{A.9}
$$

and the phase is encoded as $\beta_n(\theta)=2n\theta$, with $n=1,\ldots,\infty$. The corresponding probability reads $p_n=2r^{-1}e^{-|\alpha|^2}|\alpha|^{2n}/n!$. As shown in figure A1(d), though the spectrum of $\hat{G}$ is boundless, p_n is centered with mean particle number, which induces a finite QFI. We mention that α is generally a complex number. It brings a n-dependent phase to nth qubit, making $|\mathrm{ECS}\rangle_\theta$ generally a non-PSS.

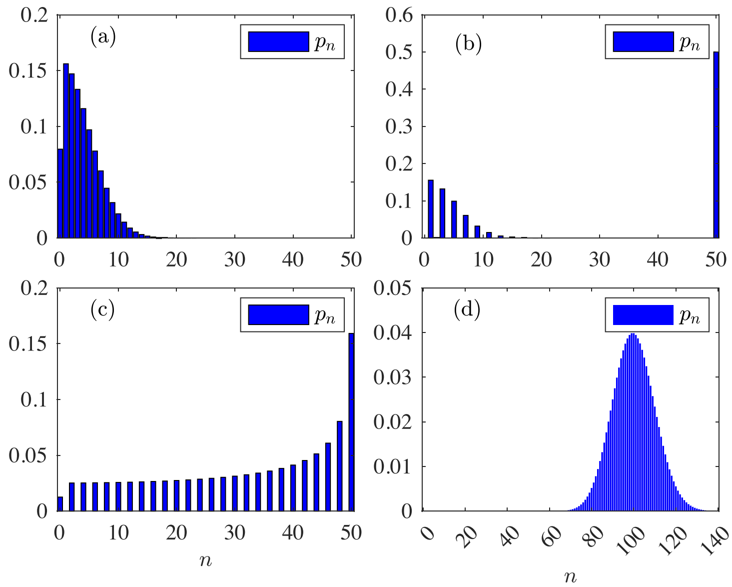

Figure A1. Probability distribution over qubits of the exemplified ESs. (a) Spin coherent state with particle number $N = 100$. (b) One-axis twisting spin squeezed state with $N = 100$, $\mu = \pi/2$, and $\nu = \pi/2$. (c) Twin Fock state with the total particle number $2N = 100$. (d) Entangled coherent state with $\alpha = 10$ and the average particle number $\langle\hat{N}\rangle = 100$.

Appendix B. Engineering of Hamiltonian equation (22)

Here, we demonstrate how to engineer the Hamiltonian equation (22) in the main text with an impurity qubit immersed in a two-component condensate. The coupled qubit-system Hamiltonian consists of three parts: $H = H_\mathrm{S} + H_\mathrm{Q} + H_\mathrm{I}$, where H_S, H_Q, and H_I describe the condensate, qubit, and qubit-system coupling, respectively. Specifically, for the condensate part, we have

$$H_\mathrm{S} = \sum_{i=a,b} \int \mathrm{d}\mathbf{r}\psi_i^\dagger(\mathbf{r}) \left[\frac{\mathbf{p}^2}{2m_\mathrm{S}} + \mathcal{E}_i + V_\mathrm{S}(\mathbf{r}) + \frac{1}{2}\frac{4\pi\hbar^2 a_{ii}}{m_\mathrm{S}}\psi_i^\dagger(\mathbf{r})\psi_i(\mathbf{r})\right]\psi_i(\mathbf{r}) + \frac{4\pi\hbar^2 a_{ab}}{m_\mathrm{S}} \int \mathrm{d}\mathbf{r}\psi_a^\dagger(\mathbf{r})\psi_b^\dagger(\mathbf{r})\psi_b(\mathbf{r})\psi_a(\mathbf{r}), \tag{B.1}$$

where $\psi_i(\mathbf{r})$ is the field operator for the atoms in ith mode, $\mathcal{E}_i$ is the energy of the ith mode, m_S is the mass of the atom, $V_\mathrm{S}(\mathbf{r})$ the external potential for condensate atoms, a_{ii} the intra-species scattering lengths, and a_{ab} the inter-species scattering length. For simplicity, we assume that $\mathcal{E}_a = \mathcal{E}_b = \mathcal{E}$ and $a_{ij} = a_\mathrm{S}$ for any i and j. The field operators are then simplified to $\psi_a(\mathbf{r}) = \psi(\mathbf{r})\hat{a}$ and $\psi_b(\mathbf{r}) = \psi(\mathbf{r})\hat{b}$ with $\psi(\mathbf{r})$ being the mode function. The condensate Hamiltonian now reduces to

$$H_\mathrm{S} = (\mathcal{E}' - g)N + gN^2 \tag{B.2}$$

where $N = \hat{a}^\dagger\hat{a} + \hat{b}^\dagger\hat{b}$ is the total particle number operator, $\mathcal{E}' = \int \mathrm{d}\mathbf{r}\psi^*(\mathbf{r})\left[\mathbf{p}^2/(2m_\mathrm{S}) + \mathcal{E} + V_\mathrm{S}(\mathbf{r})\right]\psi(\mathbf{r})$, and $g = (4\pi\hbar^2 a_\mathrm{S}/m_\mathrm{S})\int \mathrm{d}\mathbf{r}|\psi(\mathbf{r})|^4$.

Next, we turn to consider the qubit Hamiltonian, which is simply

$$H_\mathrm{Q} = \sum_{\sigma=e,g} \int \mathrm{d}\mathbf{r}\phi_\sigma^\dagger(\mathbf{r}) \left[\frac{\mathbf{p}^2}{2m_\mathrm{Q}} + \varepsilon_\sigma + V_\mathrm{Q}(\mathbf{r})\right]\phi_\sigma(\mathbf{r}), \tag{B.3}$$

where $\phi_\sigma(\mathbf{r})$ is the field operators for the excited (e) and ground (g) states, ε_σ are the corresponding energies, m_Q is the mass of the impurity atom, and $V_\mathrm{Q}(\mathbf{r})$ is the confining potential. Generally, the trapping potential for the impurity atom is very tight such that the center of mass motion of the qubit is frozen to the ground state of V_Q, say $\phi(\mathbf{r})$. The qubit Hamiltonian then reduces to

$$H_\mathrm{Q} = \varepsilon_e'|e\rangle\langle e| + \varepsilon_g'|g\rangle\langle g|, \tag{B.4}$$

where $\varepsilon_\sigma' = \int \mathrm{d}\mathbf{r}\phi^*(\mathbf{r})\left[\mathbf{p}^2/(2m_\mathrm{Q}) + \varepsilon_\sigma + V_\mathrm{Q}(\mathbf{r})\right]\phi(\mathbf{r})$.

Finally, for the qubit-system coupling, we assume that only the exited state of the qubit interacts with the condensate atom in mode b with a scattering length is a_{eb}. Therefore, the interaction Hamiltonian is

$$H_{\mathrm{I}} = \frac{2\pi\hbar^2 a_{eb}}{\bar{m}} \int d\mathbf{r}\psi_b^\dagger(\mathbf{r})\phi_e^\dagger(\mathbf{r})\phi_e(\mathbf{r})\psi_b(\mathbf{r}) = \chi_{\mathrm{qs}}|e\rangle\langle e|\hat{b}^\dagger\hat{b}, \tag{B.5}$$

where $\bar{m} = m_{\mathrm{S}}m_{\mathrm{Q}}/(m_{\mathrm{S}}+m_{\mathrm{Q}})$ is the reduced mass and $\chi_{\mathrm{qs}} = (2\pi\hbar^2 a_{eb}/\bar{m})\int \mathrm{d}\mathbf{r}|\psi(\mathbf{r})|^2|\phi(\mathbf{r})|^2$.

Now put everything back together, we have

$$H = (\mathcal{E}' - g)N + gN^2 + \varepsilon_e'|e\rangle\langle e| + \varepsilon_g'|g\rangle\langle g| + \chi_{\mathrm{qs}}|e\rangle\langle e|\hat{b}^\dagger\hat{b}. \tag{B.6}$$

After dropping the constant N and N^2 terms and setting ε_g' as the zero energy, we have

$$H_{\mathrm{qs}} = \hbar\omega_{\mathrm{q}}|e\rangle\langle e| + \chi_{\mathrm{qs}}|e\rangle\langle e|\hat{b}^\dagger\hat{b}. \tag{B.7}$$

ORCID iD

Hai-Jun Xing https://orcid.org/0000-0002-0078-2941

References

[1] Helstrom C W 1976 *Quantum Detection and Estimation Theory* (Academic)
[2] Holevo A S 1982 *Probabilistic and Statistical Aspects of Quantum Theory* (North-Holland)
[3] Giovannetti V, Lloyd S and Maccone L 2004 Quantum-enhanced measurements: beating the standard quantum limit *Science* **306** 1330–6
[4] Giovannetti V, Lloyd S and Maccone L 2006 Quantum metrology *Phys. Rev. Lett.* **96** 010401
[5] Giovannetti V, Lloyd S and Maccone L 2011 Advances in quantum metrology *Nat. Photon.* **5** 222–9
[6] Holland M J and Burnett K 1993 Interferometric detection of optical phase shifts at the Heisenberg limit *Phys. Rev. Lett.* **71** 1355
[7] Dunningham J A, Burnett K and Barnett S M 2002 Interferometry below the standard quantum limit with Bose-Einstein condensates *Phys. Rev. Lett.* **89** 150401
[8] Sanders B C 1992 Entangled coherent states *Phys. Rev.* A **45** 6811
[9] Joo J, Munro W J and Spiller T P 2011 Quantum metrology with entangled coherent states *Phys. Rev. Lett.* **107** 083601
[10] Sanders B C 2012 Review of entangled coherent states *J. Phys. A: Math. Theor.* **45** 244002
[11] Caves C M 1981 Quantum-mechanical noise in an interferometer *Phys. Rev.* D **23** 1693–708
[12] Ma J, Wang X, Sun C P and Nori F 2011 Quantum spin squeezing *Phys. Rep.* **509** 89–165
[13] Kitagawa M and Ueda M 1993 *Phys. Rev.* A **47** 5138
[14] Ulam-Orgikh D and Kitagawa M 2001 Spin squeezing and decoherence limit in Ramsey spectroscopy *Phys. Rev.* A **64** 052106
[15] Cox K C, Greve G P, Weiner J M and Thompson J K 2016 Deterministic squeezed states with collective measurements and feedback *Phys. Rev. Lett.* **116** 093602
[16] Wang M, Qu W, Li P, Bao H, Vuletić V and Xiao Y 2017 Two-axis-twisting spin squeezing by multipass quantum erasure *Phys. Rev.* A **96** 013823
[17] Pezzé L, Smerzi A, Oberthaler M K, Schmied R and Treutlein P 2018 Quantum metrology with nonclassical states of atomic ensembles *Rev. Mod. Phys.* **90** 035005 and references therein
[18] Degen C L, Reinhard F and Cappellaro P 2017 *Rev. Mod. Phys.* **89** 035002 and references therein
[19] Lee C, Huang J, Deng H, Dai H and Xu J 2012 Nonlinear quantum interferometry with Bose condensed atoms *Front. Phys.* **7** 109–30 and references therein
[20] Kitching J, Knappe S and Donley E A 2011 Atomic sensors—a review *IEEE Sens. J.* **11** 1749 and references therein
[21] Dowling J P 2008 Quantum optical metrology—the lowdown on high-N00N states *Contemp. Phys.* **49** 125–43 and references therein
[22] Monz T, Schindler P, Barreiro J T, Chwalla M, Nigg D, Coish W A, Harlander M, Hänsel W, Hennrich M and Blatt R 2011 14-qubit entanglement: creation and coherence *Phys. Rev. Lett.* **106** 130506
[23] Zou Y-Q, Wu L-N, Liu Q, Luo X-Y, Guo S-F, Cao J-H, Tey M K and You L 2018 Beating the classical precision limit with spin-1 Dicke states of more than 10,000 atoms *Proc. Natl Acad. Sci.* **115** 6381–5
[24] Louchet-Chauvet A, Appel J, Renema J J, Oblak D, Kjaergaard N and Polzik E S 2010 Entanglement-assisted atomic clock beyond the projection noise limit *New J. Phys.* **12** 065032
[25] Leroux I D, Schleier-Smith M H and Vuletić V 2010 Orientation-dependent entanglement lifetime in a squeezed atomic clock *Phys. Rev. Lett.* **104** 250801
[26] Hosten O, Engelsen N J, Krishnakumar R and Kasevich M A 2016 Measurement noise 100 times lower than the quantum-projection limit using entangled atoms *Nature* **529** 505–8
[27] Kessler E M, Kómár P, Bishof M, Jiang L, Sørensen A S, Ye J and Lukin M D 2014 Heisenberg-limited atom clocks based on entangled qubits *Phys. Rev. Lett.* **112** 190403
[28] Kruse I *et al* 2016 Improvement of an atomic clock using squeezed vacuum *Phys. Rev. Lett.* **117** 143004
[29] Sewell R J, Koschorreck M, Napolitano M, Dubost B, Behbood N and Mitchell M W 2012 Magnetic sensitivity beyond the projection noise limit by spin squeezing *Phys. Rev. Lett.* **109** 253605
[30] Ockeloen C F, Schmied R, Riedel M F and Treutlein P 2013 Quantum metrology with a scanning probe atom interferometer *Phys. Rev. Lett.* **111** 143001

[31] Muessel W, Strobel H, Linnemann D, Hume D B and Oberthaler M K 2014 Scalable spin squeezing for quantum-enhanced magnetometry with Bose-Einstein condensates *Phys. Rev. Lett.* **113** 103004
[32] Mossman M E, Corbin R A, Forbes M M and Engels P 2023 Atom interferometric imaging of differential potentials using an atom laser *Phys. Rev. Lett.* **130** 263402
[33] Rosi G, Sorrentino F, Cacciapuoti L, Prevedelli M and Tino G M 2014 Precision measurement of the Newtonian gravitational constant using cold atoms *Nature* **510** 518–21
[34] Stray B *et al* 2022 Quantum sensing for gravity cartography *Nature* **602** 590–4
[35] Kimble H J, Levin Y, Matsko A B, Thorne K S and Vyatchanin S P 2001 Conversion of conventional gravitational-wave interferometers into quantum nondemolition interferometers by modifying their input and/or output optics *Phys. Rev.* D **65** 022002
[36] The LIGO Scientific Collaboration 2011 A gravitational wave observatory operating beyond the quantum shot-noise limit *Nat. Phys.* **7** 962–5
[37] Aasi J *et al* (The LIGO Scientific Collaboration) 2013 Enhanced sensitivity of the LIGO gravitational wave detector by using squeezed states of light *Nat. Photon.* **7** 613–9
[38] Tse M *et al* 2019 Quantum-enhanced advanced LIGO detectors in the era of gravitational-wave astronomy *Phys. Rev. Lett.* **123** 231107
[39] Braunstein S L and Caves C M 1994 Statistical distance and the geometry of quantum states *Phys. Rev. Lett.* **72** 3439–43
[40] Braunstein S L, Caves C M and Milburn G J 1996 Generalized uncertainty relations: theory, examples and Lorentz invariance *Ann. Phys., NY* **247** 135–73
[41] Berry D W and Wiseman H M 2000 Optimal states and almost optimal adaptive measurements for quantum interferometry *Phys. Rev. Lett.* **85** 5098–101
[42] Huang Z, Motes K R, Anisimov P M, Dowling J P and Berry D W 2017 Adaptive phase estimation with two-mode squeezed vacuum and parity measurement *Phys. Rev.* A **95** 053837
[43] Gerry C C and Mimih J 2010 The parity operator in quantum optical metrology *Contemp. Phys.* **51** 497–511
[44] Chiruvelli A and Lee H 2011 Parity measurements in quantum optical metrology *J. Mod. Opt.* **58** 945–53
[45] Bollinger J J, Itano W M, Wineland D J and Heinzen D J 1996 Optimal frequency measurements with maximally correlated states *Phys. Rev.* A **54** R4649–52
[46] Gerry C C 2000 Heisenberg-limit interferometry with four-wave mixers operating in a nonlinear regime *Phys. Rev.* A **61** 043811
[47] Gerry C C and Campos R A 2001 Generation of maximally entangled photonic states with a quantum-optical Fredkin gate *Phys. Rev.* A **64** 063814
Gerry C C and Campos R A 2002 *Phys. Rev.* A **65** 039902(E)
[48] Anisimov P M, Raterman G M, Chiruvelli A, Plick W N, Huver S D, Lee H and Dowling J P 2010 Quantum metrology with two-mode squeezed vacuum: parity detection beats the Heisenberg limit *Phys. Rev. Lett.* **104** 103602
[49] Seshadreesan K P, Anisimov P M, Lee H and Dowling J P 2011 Parity detection achieves the Heisenberg limit in interferometry with coherent mixed with squeezed vacuum light *New J. Phys.* **13** 083026
[50] Ouyang Y, Wang S and Zhang L 2016 Quantum optical interferometry via the photon-added two-mode squeezed vacuum states *J. Opt. Soc. Am.* B **33** 1373
[51] Lee H, Kok P and Dowling J P 2002 A quantum Rosetta stone for interferometry *J. Mod. Opt.* **49** 2325–38
[52] Pezzé L and Smerzi A 2008 Mach-Zehnder interferometry at the Heisenberg limit with coherent and squeezed-vacuum light *Phys. Rev. Lett.* **100** 073601
[53] Pezzé L and Smerzi A 2013 Ultrasensitive two-mode interferometry with single-mode number squeezing *Phys. Rev. Lett.* **110** 163604
[54] Krischek R, Schwemmer C, Wieczorek W, Weinfurter H, Hyllus P, Pezzé L and Smerzi A 2011 Useful multiparticle entanglement and sub-shot-noise sensitivity in experimental phase estimation *Phys. Rev. Lett.* **107** 080504
[55] Zhong W, Huang Y, Wang X and Zhu S-L 2017 Optimal conventional measurements for quantum-enhanced interferometry *Phys. Rev.* A **95** 052304
[56] Hofmann H F 2009 All path-symmetric pure states achieve their maximal phase sensitivity in conventional two-path interferometry *Phys. Rev.* A **79** 033822
[57] Yurke B, McCall S L and Klauder J R 1986 SU(2) and SU(1,1) interferometers *Phys. Rev.* A **33** 4033–54
[58] Lee C 2006 Adiabatic Mach-Zehnder interferometry on a quantized Bose-Josephson junction *Phys. Rev. Lett.* **97** 150402
[59] Tacla A B, Boixo S, Datta A, Shaji A and Caves C M 2010 Nonlinear interferometry with Bose-Einstein condensates *Phys. Rev.* A **82** 053636
[60] Gross C, Zibold T, Nicklas E, Estève J and Oberthaler M K 2010 Nonlinear atom interferometer surpasses classical precision limit *Nature* **464** 1165–9
[61] Xing H, Wang A, Tan Q-S, Zhang W and Yi S 2016 Heisenberg-scaled magnetometer with dipolar spin-1 condensates *Phys. Rev.* A **93** 043615
[62] Boixo S, Flammia S T, Caves C M and Geremia J 2007 Generalized limits for single-parameter quantum estimation *Phys. Rev. Lett.* **98** 090401
[63] Gammelmark S and Mølmer K 2011 Phase transitions and Heisenberg limited metrology in an Ising chain interacting with a single-mode cavity field *New J. Phys.* **13** 053035
[64] Marzolino U and Prosen T 2014 Quantum metrology with nonequilibrium steady states of quantum spin chains *Phys. Rev.* A **90** 062130
[65] Boyajian W L, Skotiniotis M, Dür W and Kraus B 2016 Compressed quantum metrology for the Ising Hamiltonian *Phys. Rev.* A **94** 062326
[66] Liu R, Chen Y, Jiang M, Yang X, Wu Z, Li Y, Yuan H, Peng X and Du J 2021 Experimental critical quantum metrology with the Heisenberg scaling *npj Quantum Inf.* **7** 170
[67] Fisher R 1923 On the dominance ratio *Proc. R. Soc. Edinburgh* **42** 321–314
Fisher R 1925 Theory of statistical estimation *Proc. Camb. Phil. Soc.* **22** 700–25
[68] Viola L, Knill E and Lloyd S 1999 Dynamical decoupling of open quantum systems *Phys. Rev. Lett.* **82** 2417
[69] Gong Z R and Yao W 2013 Protecting dissipative quantum state preparation via dynamical decoupling *Phys. Rev.* A **87** 032314
[70] Huang J, Huo H, Zhuang M and Lee C 2022 Efficient generation of spin cat states with twist-and-turn dynamics via machine optimization *Phys. Rev.* A **105** 062456

[71] Gerry C C, Benmoussa A and Campos R A 2005 Quantum nondemolition measurement of parity and generation of parity eigenstates in optical fields *Phys. Rev.* A **72** 053818
[72] Sun L *et al* 2014 Tracking photon jumps with repeated quantum non-demolition parity measurements *Nature* **511** 444–8
[73] Cohen J, Smith W C, Devoret M H and Mirrahimi M 2017 Degeneracy-preserving quantum nondemolition measurement of parity-type observables for cat qubits *Phys. Rev. Lett.* **119** 060503
[74] Hu L *et al* 2019 Quantum error correction and universal gate set operation on a binomial bosonic logical qubit *Nat. Phys.* **15** 503–8
[75] Ni Z *et al* 2023 Beating the break-even point with a discrete-variable-encoded logical qubit *Nature* **616** 56–60